Praise Worthy Prize

International Review of Chemical Engineering (I.RE.CH.E.), Vol. 5, N. 3
ISSN 2035-1755 *May 2013*

Stereoscopic Particle Image Velocimetry Analysis of Air-Water Flow in a Pipe Separator

Eyitayo A. Afolabi, J. G. M. Lee

Abstract – *Experimental investigations have been carried out to study the hydrodynamic flow behaviour and phase separation of air-water flow in a pipe separator. Stereoscopic particle image velocimetry measurements are conducted at three different axial positions for air-water mixture at a constant air flow rate of 4.5×10^{-3} m^3/s and six different water flow rates. Effects of air flow in the air-water flow field are investigated by comparing the velocity distributions of air–water flow with that of only water flow field. Experimental results indicate that the tangential and radial velocity flow patterns of air-water flow and water flow were the same. However, the magnitudes of the velocity profiles for air-water were greater than that of only water flow fields. The axial velocity profiles illustrated the phase separation that occurred as air-water flow through the pipe separator.*

Keywords*: Flow Pattern, Particle Image Velocimetry, Pipe Separator, Turbulence*

Nomenclature

d	Pipe diameter (m)
U_G	Gas superficial velocity (ms^{-1})
U_L	Liquid superficial velocity (ms^{-1})
ρ_G	Gas phase density (kgm^{-3})
ρ_L	Liquid phase density (kgm^{-3})
μ_L	Liquid phase viscosity (Pa s)
$(\Delta P/_L)$	Frictional pressure drop (Pa m^{-1})

I. Introduction

Particle Image Velocimetry (PIV) has been increasingly employed in experimental fluid mechanics over the past 2 decades, following progresses in imaging and illumination devices as well as in post-processing algorithms.

It is a robust optically-based measurement technique for measuring the whole instantaneous flow field without contacting the flow. PIV relies on the basic principle of distance over time to yield velocity, typically along a two-dimensional slice within a particular flow [1]. PIV is different from the laser Doppler anemometry (LDA) technique, in that with LDA only one point in the flow is probed. However, PIV determined the simultaneous velocity at many points in the flow.

Stereoscopic particle image velocimetry (SPIV) is an extension of conventional 2-D PIV for measuring the third velocity component in the laser light sheet plane.

The determination of the velocity of a fluid using SPIV consists of a number of separate processes namely:

- Tracer particles that are assumed to strictly follow the fluid dynamics (the degree to which the particles faithfully follow the flow is represented by the Stokes number) are added to the flow [2]-[3].
- At least two cameras are to be used to view a flow field from different perspective positions.
- A laser beam illuminates a plane of the flow under investigation twice within a short time interval.
- The test section is enclosed within a clear water prism in order to minimize the effect of refraction [4] - [5].
- The laser light is scattered by tracer particles and recorded in a sequence of frames using equipment such as a CCD camera, photographic film or holographic plates.
- Computer hardware with suitable software is used to process the recorded images and extract velocity information indirectly through the tracer particles.
- The calibration of the camera is achieved using a target mounted on an accurate traversing mechanism. The calibration images are then used to map locations between the fluid and the cameras and also to calculate the local magnification factor [5].
- The combination of a set of 2-dimensional vector fields from a pair of cameras is used to obtain a three dimensional vector field.

The PIV technique has been successfully used to obtain measurements of single phase flow velocity fields [6], and it can be extended to multiphase flows in order to obtain full field velocity measurements for each phase.

Simultaneous measurements of the continuous and dispersed phases are extremely important in order to understand inter-phase interaction and the concentrations, sizes and shapes of the dispersed phases.

The PIV measurement of a multiphase flow is more complicated than that of a single phase, and this is due to the presence of dispersed phases that introduce the

Manuscript received and revised April 2013, accepted May 2013

following additional problems:

(a) Strong reflection at interfaces between the phases (particularly gas-liquid interfaces).
(b) In the region on the PIV image where the concentration of the dispersed phase is rather high, there is little space left for the tracer particles, resulting in low valid detection probability.
(c) The dispersed phase can introduce shadows, which together with the dispersed phase in front of the light plane hamper visibility in the measurement plane. This reduces the amount of information present in the PIV images.
(d) The deformation of the dispersed phase, such as gas bubbles, during the time delay between the recordings of flow may reduce the precision of PIV measurement, and lastly,
(e) The different refractive indices of the phases.

When the conventional PIV system is used for the measurement of a multiphase flow such as a bubbly flow, the intensity of light reflected from the surfaces of bubbles not only saturates the CCD camera but also overwhelms the intensity of light refracted from the seeding particles for PIV in its vicinity [7].

The continuous phase can be differentiated from the dispersed phase by using fluorescent dyes and optical band pass filters. For example, the combination of the PIV technique with laser induced fluorescence (LIF) and/or the shadow image technique (SIT) are options available to measure the velocity distributions of the phases and their interaction [8]-[9]. Nevertheless, PIV measurement techniques are limited to relatively low volume fractions (usually $\propto \leq$ 5%) of the dispersed phase [10]-[11]. Nowadays, compact separators are widely used as an effective and economical alternative to conventional separators especially in offshore platforms in oil and gas production operations. The compact separator is simpler to operate, more lightweight, has neither moving nor internal parts, requires less floor space, and involves lower capital and operational costs. A pipe separator is a device that spins a continuous phase stream in order to remove entrained dispersed phases by centrifugal force [12]. As in [13], experimental study and mechanistic modelling were conducted to ascertain the separation performance of the three phase cylindrical cyclone as a device that effects the partial separation of air-water-oil mixtures at moderate velocities. However, the cylindrical cyclone performs as a mixer rather than separator at high velocities. There is a lack of detailed analysis of the complex 3D flow field in the three phase pipe separator in the literature and this prevents complete confidence in its design. Thus, the need for additional research which the present work seeks to provide. The objective of the work is threefold: to investigate complex flow behaviour, provide SPIV measurement results that can be used to validate air-water two-phase Computational Fluid Dynamic (CFD) simulations, and to assess the phase separation of air-water flow in a pipe separator. A detailed investigation of hydrodynamic flow behaviour will allow the correct prediction of separation performance, which is necessary for appropriate design in all applications.

II. Experimental Facility and Procedure

II.1. Experimental Facility

The multiphase flow facility used in this study is based on one of the geometries developed for multiphase flow separation by the Separation Technology Project of the University of Tulsa, USA [13].

A 30 mm ID laboratory prototype gas-liquid-liquid cylindrical cyclone (GLLCC) / pipe separator was fabricated and installed in the School of Chemical Engineering and Advanced Materials, Newcastle University, UK to investigate the hydrodynamic flow behaviour of multiphase flow under different flow conditions at atmospheric pressure and room temperature [14]. The experiments are performed using water (density 996 kg/m^3, viscosity 0.001 kg/ms) and air (density 1.225 kg/m^3, viscosity 0.000018 kg/ms) at room temperature and atmospheric outlet pressure.

Water and air are pumped from their respective storage tanks, metered and introduced to the pipe separator via an inline mixer, which ensures minimum mixing. The test section was constructed using a transparent perspex tube and the main body is a 30 mm ID vertical cylinder with a height of 1675 mm. The inlet is a 30-mm ID pipe, inclined at an angle of 27 degrees from the horizontal and connected tangentially at 585 mm from the top of the vertical main body. The inlet configuration was constructed by inserting a gradually reduced inlet nozzle designed by narrowing the inlet down from a full bore cross sectional area to 25% of the inlet cross sectional area. The flow from the three outlets was controlled using natural rubber bungs to specify the split ratio as a function of mass flow rate passing through each outlet. Detailed drawing of the pipe separator test section is given in Fig. 1.

II.2. Separation Mechanism

The air-water mixture enters the pipe separator through the inclined inlet designed to promote the pre-separation of the gas-liquid mixture. The tangential inlet with reduced area produces a swirling motion in the vertical cylindrical pipe. Due to the differences in density, the centrifugal effect segregates the air-water mixture, thereby allows air to flow upward and leaves through the gas outlet. In addition, water flow to the lower section of the pipe separator and flow out through the water and oil-rich outlets.

II.3. Air-Water flow Experiment

As a result of the nozzle inserted at the inlet junction of the pipe separator, the swirling motion of the segregated flow changes to different flow patterns away from the inlet section.

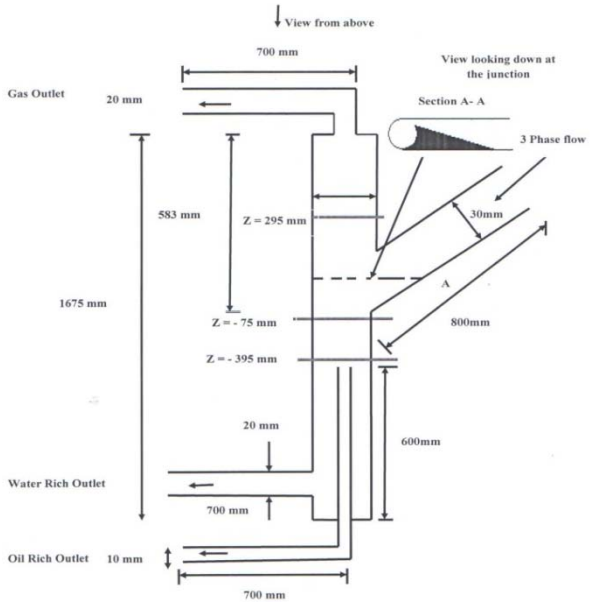

Fig. 1. Three-Phase Pipe Separator System

TABLE I
FLOW RATES FOR AIR-WATER EXPERIMENTS

	Gas flow rate ($10^{-5}m^3/s$)	Water flow rate ($10^{-4}m^3/s$)	Gas volume fraction (%)	Split ratio (water outlet)	Split ratio (air outlet)	Split ratio (oil outlet)
A	4.5	2.05	18 .0	0.317	0.066	0.617
B	4.5	1.96	18.67	0.332	0.069	0.599
C	4.5	1.85	19.57	0.352	0.072	0.576
D	4.5	1.58	22.17	0.40	0.1	0.5
E	4.5	1.48	23.32	0.439	0.1	0.47
F	4.5	1.32	25.42	0.48	0.11	0.41

During regular operation, a bubble, slug, churn or annular flow pattern is established inside the main body of the pipe separator [15]. Preliminary investigations by Vazquez [13] concluded that cylindrical cyclone achieves more efficient separation with stratified flow pattern at the inclined inlet. Therefore, this investigation considered stratified wavy flow pattern of air-water mixture at the inclined inlet of the pipe separator.

At atmospheric pressure and room temperature, a stratified wavy flow pattern at the inlet section of the separator was observed with air flow rate of $0.000045 m^3/s$. This air flow rate and corresponding water flow rates shown in Table I with their associated properties such as densities, viscosities e.t.c, were then used to calculate and plot the Martinelli (X), and Taitel and Dukler (K) parameters onto the air-water flow map for inclined pipe [16]-[17]. These parameters were observed to lie in the stratified wavy region and confirmed a segregated flow pattern occurring at the inlet section of the pipe separator:

$$X = \sqrt{\frac{\left(\Delta P/_L\right)L}{\left(\Delta P/_G\right)G}} \quad (1)$$

$$K = \frac{U_G^2}{dgcos\alpha}\left(\frac{\rho_G}{\rho_G - \rho_L}\right)\left(\frac{\rho_L d U_L}{\mu_L}\right) \quad (2)$$

The experimental investigation of the two phases was carried out with the air volumetric flow rate kept constant at $0.000045 m^3/s$ and six different water flow rates as shown in Table I.

In order to study the effect of air flow in air-water flow field, another experiment was performed with the same water flow rate as in air-water flow measurements. In addition, the split ratio for the water rich outlet is defined as the ratio of liquid flow rate passing through the water-rich outlet to the total liquid flow rate at the inlet.

II.4. S-PIV Set-Up

The stereo-PIV system used for this investigation was manufactured by TSI Inc and loaned from the EPSRC engineering instruments pool. A CFR-200 double pulsed Nd: YAG laser system designed by Big Sky Laser was used as the light source to illuminate the tracer particles in the air-water flow under investigation with a 200 mJ per pulse laser, and each light pulse had duration of 9 ns at a wavelength of 532 nm.

As shown in Fig. 2, two TSI Model 630059 POWERVIEW TM Plus 4MP PIV cameras with CCD sensors were installed on the Scheimpflug mounts so as to satisfy the stereoscopic camera condition at an angle of $+45^o$ and -45^o to the light sheet. By tilting the image sensor plane and the lens plane to the Scheimpflug

condition, the plane best of focus could be found so that it was aligned with the light sheet [5].

These cameras were positioned at both sides of the light sheet 300 mm away from the measuring plane and then connected to a 64 bit frame grabber to capture and digitize images and communicate with a computer. A TSI 610035 laser pulse synchronizer was used to synchronize the image capturing and laser pulses.

A water prism of 45 degrees was constructed, then filled with water and moved to the test section of the experimental rig in order to minimize optical distortion arising from refraction through the perspex wall [6].

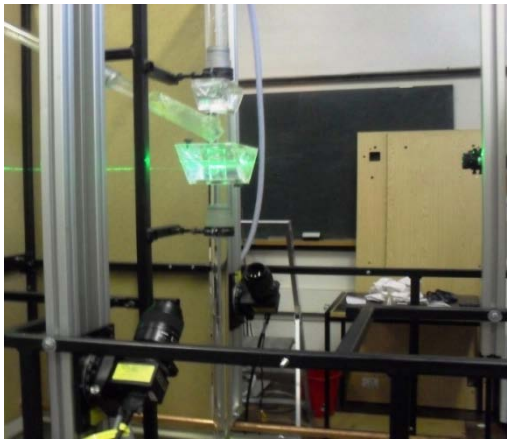

Fig. 2. S-PIV experimental set-up

The stereo-PIV set up for imaging the air-water flow field was carried out with the long wavelength pass filters fitted to the cameras in order to prevent the reflection of scattered light from the gas bubbles.

The continuous phase was seeded with 10070-3 fluorescent microsphere tracer particles (from TSI inc.) capable of absorbing light of wavelength 532 nm and emitting it at 542 nm, so that the light reflected from the tracer particles could be used to measure the velocity field of the flow under investigation. For air-water experiment, the interest is on investigating the effect of air flow on the water flow field as the phases separate within the pipe separator.

II.5. Camera Calibration

A single plane calibration target populated by a Cartesian grid of 2 mm white marker dots with a 3 mm cross at the centre on a black background was cut to size to fit into the test section. The calibration target was mounted on a flat plate and inserted into the test section to coincide exactly with the light sheet, and it was moved using a micrometer in seven steps of 0.5mm (Z=-1.5,-1,-0.5, 0, 0.5, 1, 1.5 mm). The error in the movement of the micrometer was found to be less than 0.01 mm. At each location, the stereo-cameras were set to satisfy the Scheimpflug condition and images of the target were recorded and analysed by the perspective calibration method of the INSIGHT 3G software. The calibration image analysis produced a set of calibration points used to create a calibration mapping function, which was then used to combine 2-D PIV vector fields in order to obtain the three-dimensional vector field [5].

II.6. SPIV Evaluation and Post-Processing

Two hundred pairs of images were recorded for water-air multiphase flow at three different axial positions Z= -0.395 m, -0.750 m and 0.295 m along the vertical axis of the cyclone (Fig. 1). The software INSIGHT 3G from TSI Inc was used to control the hardware, retrieve and process raw images in order to gain data on velocity vector fields. In order to evaluate the recorded images via cross-correlation, the particle image is subdivided into small interrogation windows. For each interrogation window the average particle image separation is determined by cross-correlation and localization of the correlation peak. In this work, a multi-pass processing scheme was used; consisting of two passes with interrogation windows of 64 × 64 pixels and 50% overlap.

Another pass was applied with an interrogation area of 32 × 32 pixels and 50% overlap. Erroneous vectors were removed and replaced by a global velocity filter and local 3 × 3 median filters. The outliers were finally interpolated to fill gaps in the vector fields.

Dividing with the known time between the two images captured the displacement vectors are converted into velocity vectors as follows:

$$\bar{w} = \frac{\Delta \bar{x}}{\Delta t} \tag{3}$$

where $\bar{w}$ is the velocity vector, $\bar{x}$ is the average displacement vector and $\bar{t}$ denotes the time delay between two image frames. The 2-D instantaneous vector fields were then combined using the 3-D calibration-based method to obtain the 3-D vector fields [5].

It was not possible to measure the velocity distribution of each of the phases due to the high volume fraction of air. Therefore, the conventional SPIV image processing technique was applied to the air-water flow velocity maps that cannot differentiate between each of the phases present in the air-water multiphase flow.

III. Results and Discussion

The comparison between mean velocity profiles of the air-water and water flow fields obtained by the stereo PIV technique are presented and discussed in this section. The comparison is aimed at determining the effect of air flow in air-water flow field as a way of explaining the phase separation of air-water mixture that occurred in pipe separator.

All experimental measurements at *Z*= -395 mm and –75mm presented in this paper were extracted along the *y*=0 line. However, it was not possible to extract enough data for graphical interpretation at *Z*= 295 mm along the *y*=0 section due to the conventional SPIV processing

algorithm used in this investigation (as discussed in SPIV set-up) that cannot differentiate the velocity distributions of the multiphase flow into each phase.

In addition, as air separates from the mixture and then concentrates at the upper section of the pipe separator it introduces shadows that hampers visibility. This reduces the amount of information present in the PIV images.

Therefore, contour plot of the velocity profiles are then presented at *Z*= 295 mm axial position.

III.1. Tangential Velocity

Figs. 3 and 4 compare the mean tangential velocities of the water and air-water flows at *Z*= -395 mm and - 75 mm respectively.

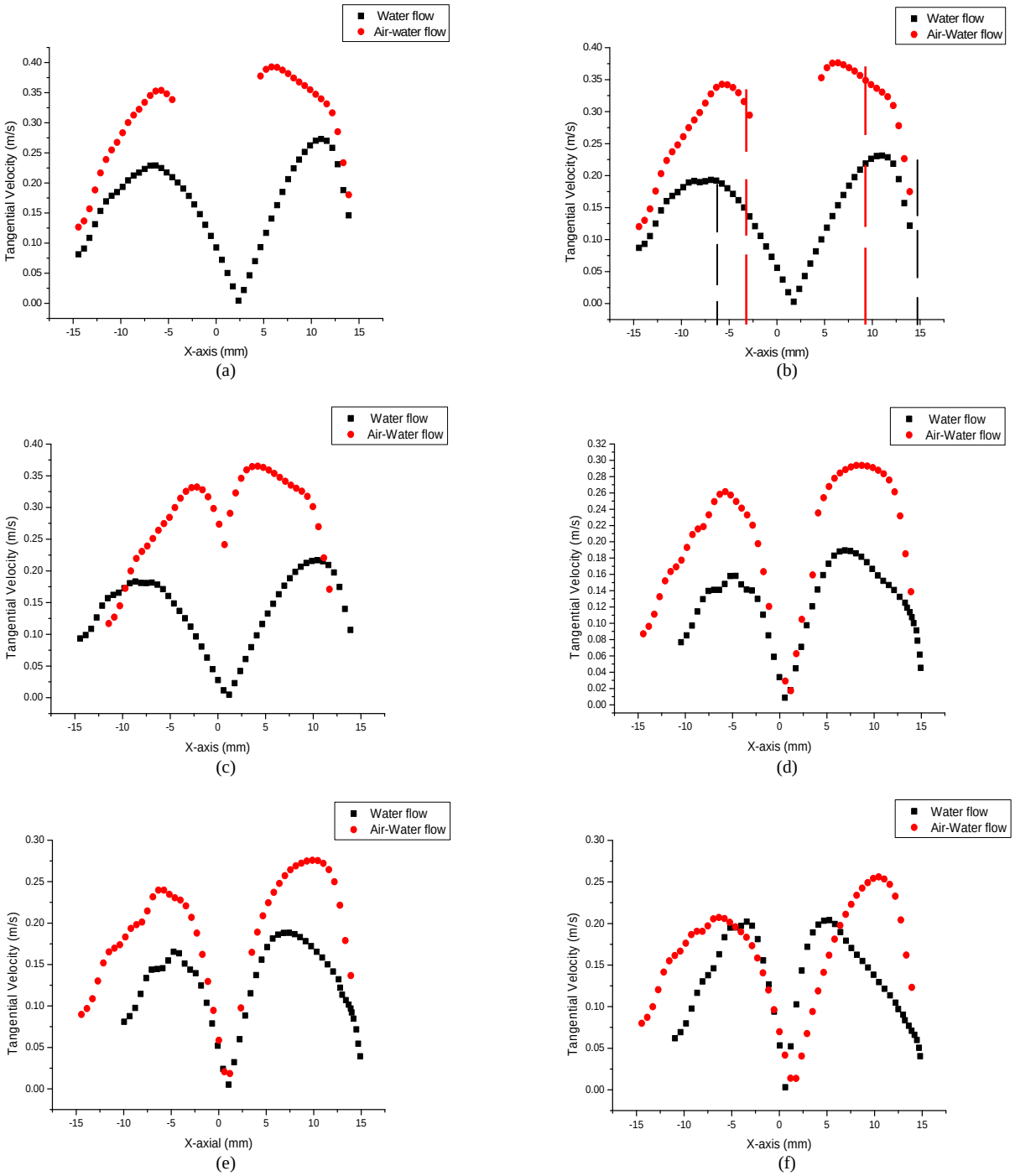

Figs. 3. Profiles of the mean tangential Velocity for water flow and air-water flow at Z= -395 mm axial position; (a): $2.05\times10^{-4}m^3/s$ (water), $4.5\times10^{-5}m^3/s$ (air); (b): $1.96\times10^{-4}m^3/s$ (water), $4.5\times10^{-5}m^3/s$ (air); (c): $1.85\times10^{-4}m^3/s$ (water), $4.5\times10^{-5}m^3/s$ (air); (d): $1.58\times10^{-4}m^3/s$ (water), $4.5\times10^{-5}m^3/s$ (air); (e): $1.48\times10^{-4}m^3/s$ (water), $4.5\times10^{-5}m^3/s$ (air); (f): $1.32\times10^{-4}m^3/s$ (water), $4.5\times10^{-5}m^3/s$ (air)

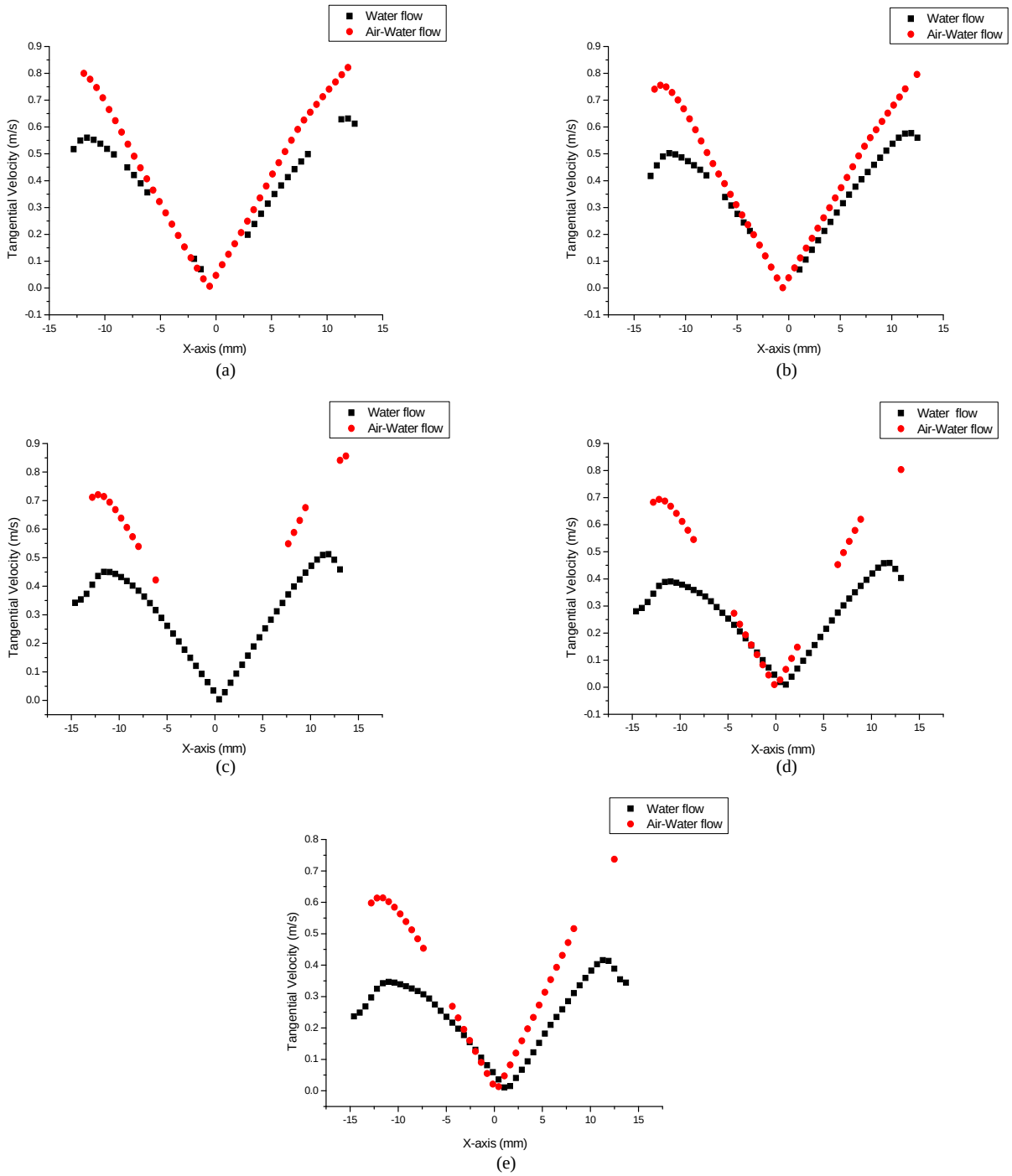

Figs. 4. Profiles of the Mean Tangential Velocity for Water Flow and Air-Water Flow at Z= -75 mm Axial Position (a): $1.96\times10^{-4}m^3/s$ (water), $4.5\times10^{-5}m^3/s$ (air); (b): $1.85\times10^{-4}m^3/s$ (water), $4.5\times10^{-5}m^3/s$ (air); (c): $1.58\times10^{-4}m^3/s$ (water), $4.5\times10^{-5}m^3/s$ (air); (d): $1.48\times10^{-4}m^3/s$ (water), $4.5\times10^{-5}m^3/s$ (air); (e): $1.32\times10^{-4}m^3/s$ (water), $4.5\times10^{-5}m^3/s$ (air)

The tangential velocity distributions of both the water and air-water flow fields increases as we move away from the centre of the tube, reaching a maximum and then rapidly decreasing close to the wall. This implies the tangential velocity profiles show a forced vortex near the centre surrounded by a free vortex at the wall of the pipe separator. Similar flow pattern have also been observed in the experimental works of Bergström, J. and Vomhoff [18], Concha [19] and Fisher and Flack [20] on velocity distributions of flow in hydrocyclone.

The magnitudes of both the free vortex and forced vortex in the air-water flow field gradually increase when compared with those of the water flow field.

Therefore, the effect of air flow on the air-water velocity field when compared with that of water alone is an increase in values of the mean tangential velocity.

This is expected, since there is an increase in the air-water flow rate when compare with that of the water flow at the inlet section of the pipe separator.

In Figs. 3, the location at which the free vortex region begins depends on the volume fraction of water. At high water volume fractions, the free vortex of the air-water flow begins at smaller values of radius. However, at lower water volume fractions, it begins at larger values of the radius. This is due to an increase in the air volume fractions associated with lower water volume fractions that cause interfacial waves and mixing at the interface. However, Figs. 4(a)-(e) show that the free vortex region begins at larger values of radius for air-water profiles in comparison with the water-only profiles. For example, Fig. 4(d) shows that the free vortex starts at x=-12.25mm for the water flow profile, but at x=-12.5mm for the measured air-water profile.

III.2. Axial Velocity

Figs. 5 show the relationship between the mean axial velocity profiles of the water and air-water flow field at Z= -75 mm.In accordance with other researchers such as in [21]-[22], the positive axial velocity profile is referred to as region of flow in an upward direction with respect to the rotation axis.

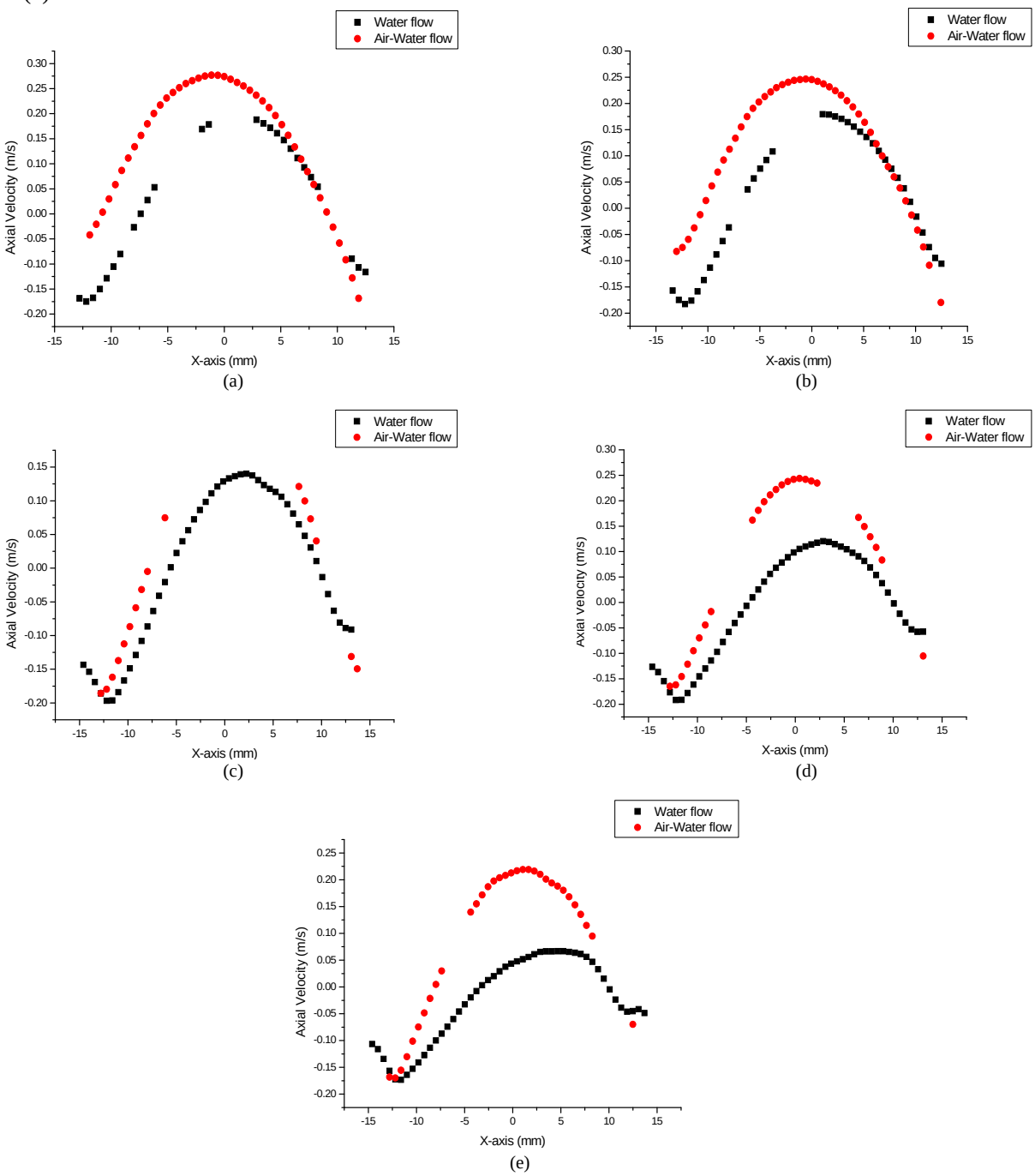

Figs. 5. Profiles of the Mean Axial Velocity for Water Flow and Air-Water Flow at Z= -75 mm Axial Position; (a): 1.96×10^{-4}m^3/s (water), 4.5×10; (b): 1.85×10^{-4}m^3/s (water), 4.5×10^{-5}m^3/s (air); (c): 1.58×10^{-4}m^3/s (water), 4.5×10^{-5}m^3/s (air); (d): 1.48×10^{-4}m^3/s (water), 4.5×10^{-5}m^3/s (air); (e): 1.32×10^{-4}m^3/s (water), 4.5×10^{-5}m^3/s (air)

While a negative axial velocity profile will be taken as a region of flow in a downward direction from the rotation axis. Figs. 6(a)-(e) reveal that the axial velocity flow profiles consist of an upward flow at the centre of the tube and a downward flow at the wall. The value of the axial velocity of the air-water flow is greater than that of the water-only flow at all x-axis coordinates. This shows that the addition of air in the air-water flow field results in an increase in the magnitude of the axial velocity profile on comparison with that of the only water flow.

III.3. Radial Velocity

Figs. 6 show a comparison between the mean radial velocity profiles of the water and water-air flows at Z= -75 mm axial position in the pipe separator.

In accordance with other researchers such as in [23], radial velocity flow is said to be directed inward when the radial velocity is negative and outward when it is positive. The radial velocity profiles of both the water and air-water flow fields are found to be directed outwards at all x-axis coordinates.

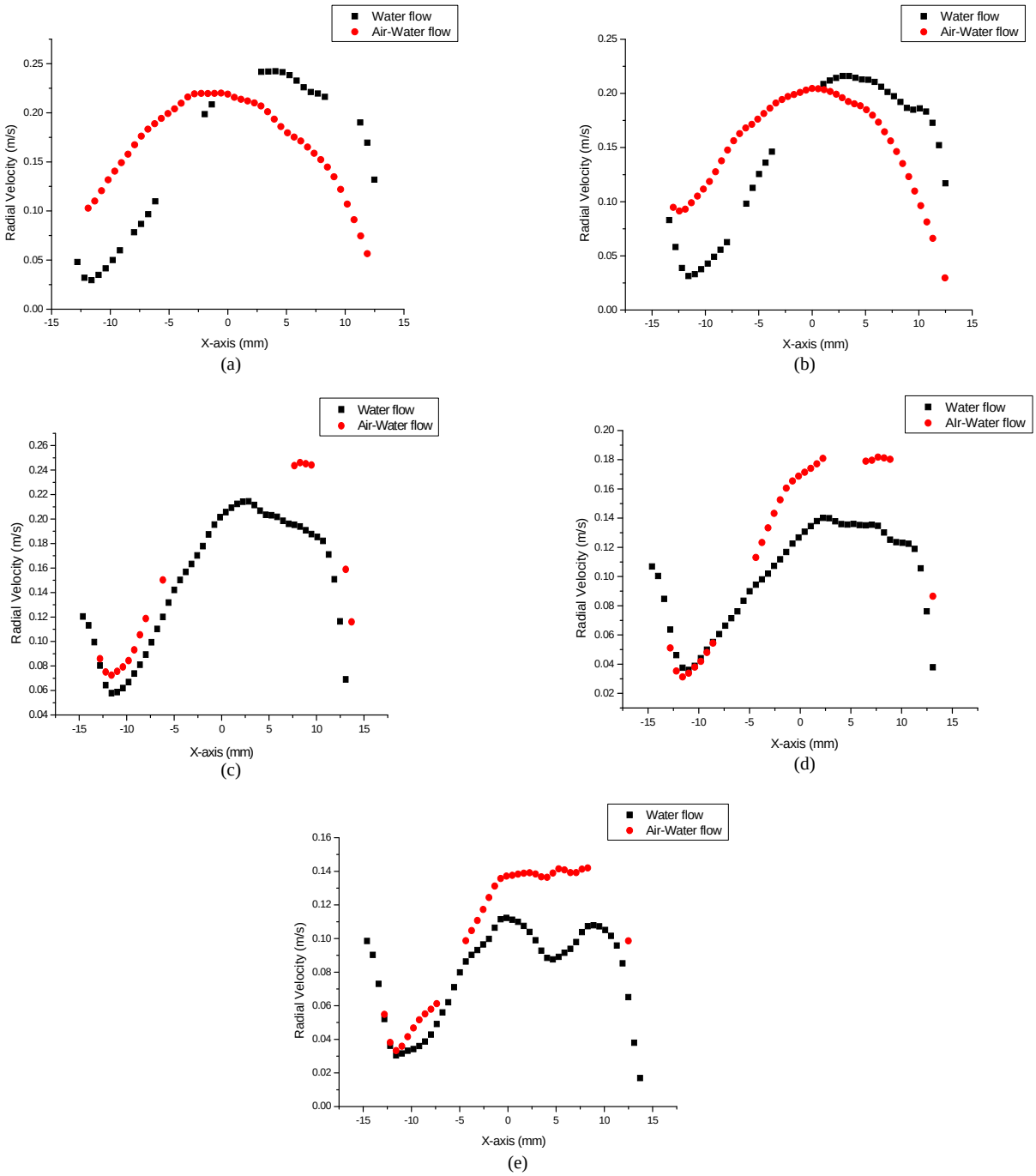

Figs. 6. Profiles of the mean radial velocity for water flow and air-water flow at Z= -75 mm axial position. (a): 1.96×10^{-4}m^3/s (water), 4.5×10^{-5}m^3/s (air); (b): 1.85×10^{-4}m^3/s (water), 4.5×10^{-5}m^3/s (air); (c): 1.58×10^{-4}m^3/s (water), 4.5×10^{-5}m^3/s (air); (d): 1.48×10^{-4}m^3/s (water), 4.5×10^{-5}m^3/s (air); (e): 1.32×10^{-4}m^3/s (water), 4.5×10^{-5}m^3/s (air)

In Figs. 6 (a)-(b), the magnitude of the radial velocity profile for the air-water flow is found to be larger than that of the water flow at negative values of *x*. However, at positive values of *x*, the magnitude of the radial velocity profile for the air-water flow is smaller than that of the water flow.

Figs. 6(c)-(e) show that the magnitude of the radial velocity profiles for the air-water flow is observed to be greater than that for the water flow as shown in Figs. 6 when moved away from the centre of the tube.

III.4. Phase Separation

The main objective of this research work is to investigate the hydrodynamic behaviour of air-water flow in a pipe separator. The SPIV measurement is aimed at explaining the partial phase separation of multiphase flow primarily designed to be achieved by the pipe separator. Figs. 7 show a noticeable difference in the flow pattern between the axial velocity contour plots of air-water flow and only water flow fields at Z= 295 mm, as most of the area in the contour plots of air-water flow field was occupied by the upward flow.

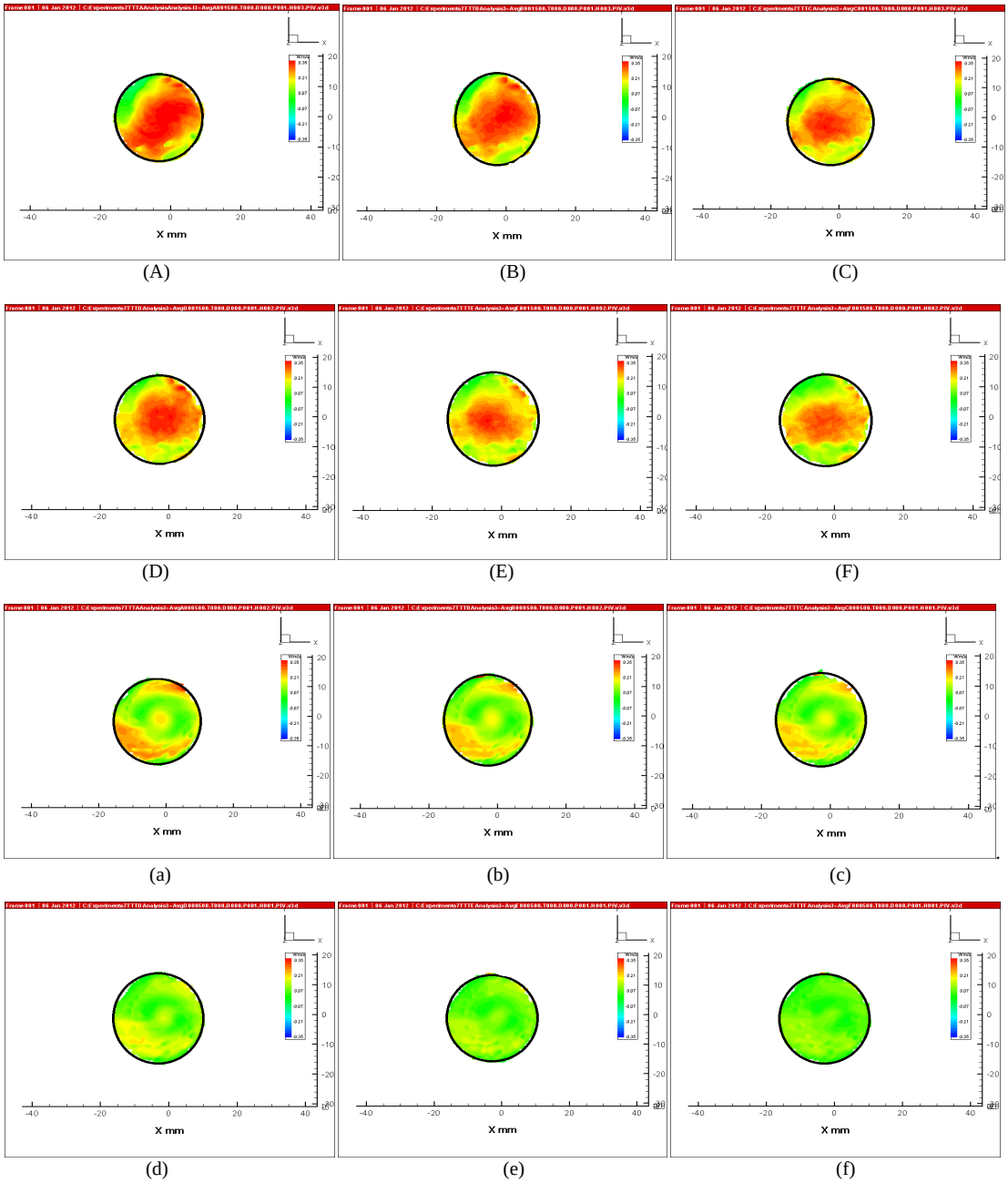

Figs. 7. Contour Plots of the Mean Axial Velocity for Water flow and Air-Water flow at *Z*= 295 mm axial position
(A): $2.05\times10^{-4}m^3/s$ (water), $4.5\times10^{-5}m^3/s$ (air); (B): $1.96\times10^{-4}m^3/s$ (water), $4.5\times10^{-5}m^3/s$ (air); (C):$1.85\times10^{-4}m^3/s$ (water), $4.5\times10^{-5}m^3/s$ (air); (D):$1.58\times10^{-4}m^3/s$ (water), $4.5\times10^{-5}m^3/s$ (air); (E): $1.48\times10^{-4}m^3/s$ (water), $4.5\times10^{-5}m^3/s$ (air); (F): $1.32\times10^{-4}m^3/s$ (water), $4.5\times10^{-5}m^3/s$ (air);)
(a): $2.05\times10^{-4}m^3/s$ (water) (b): $1.96\times10^{-4}m^3/s$ (water) (c): $1.85\times10^{-4}m^3/s$ (water) (d): $1.58\times10^{-4}m^3/s$ (water) (e): $1.48\times10^{-4}m^3/s$ (water) (f): $1.32\times10^{-4}m^3/s$ (water)

It means that the concentration of air flow in the air-water flow fields is higher than that of water flow fields at *Z*= 295 mm as most of the air flow in the air-water mixture flow separates and moves upward to flow out through the gas outlet of the pipe separator.

The investigation is helpful in order to understand the phase separation that occurred as air-water flow through the pipe separator.

In Figs. 8, there is no difference in the flow pattern of the air-water and only water flow fields at *Z*=-395 mm except the magnitude of the upward flow that increases with an increase in the flow rate at the inlet.

This observation is in agreement with the finding made by Dlamini et al; [24] that the axial velocity component is an indication of the magnitude of the two spiral flows and that it determines the volumetric distribution of the fluid between the overflow and underflow streams.

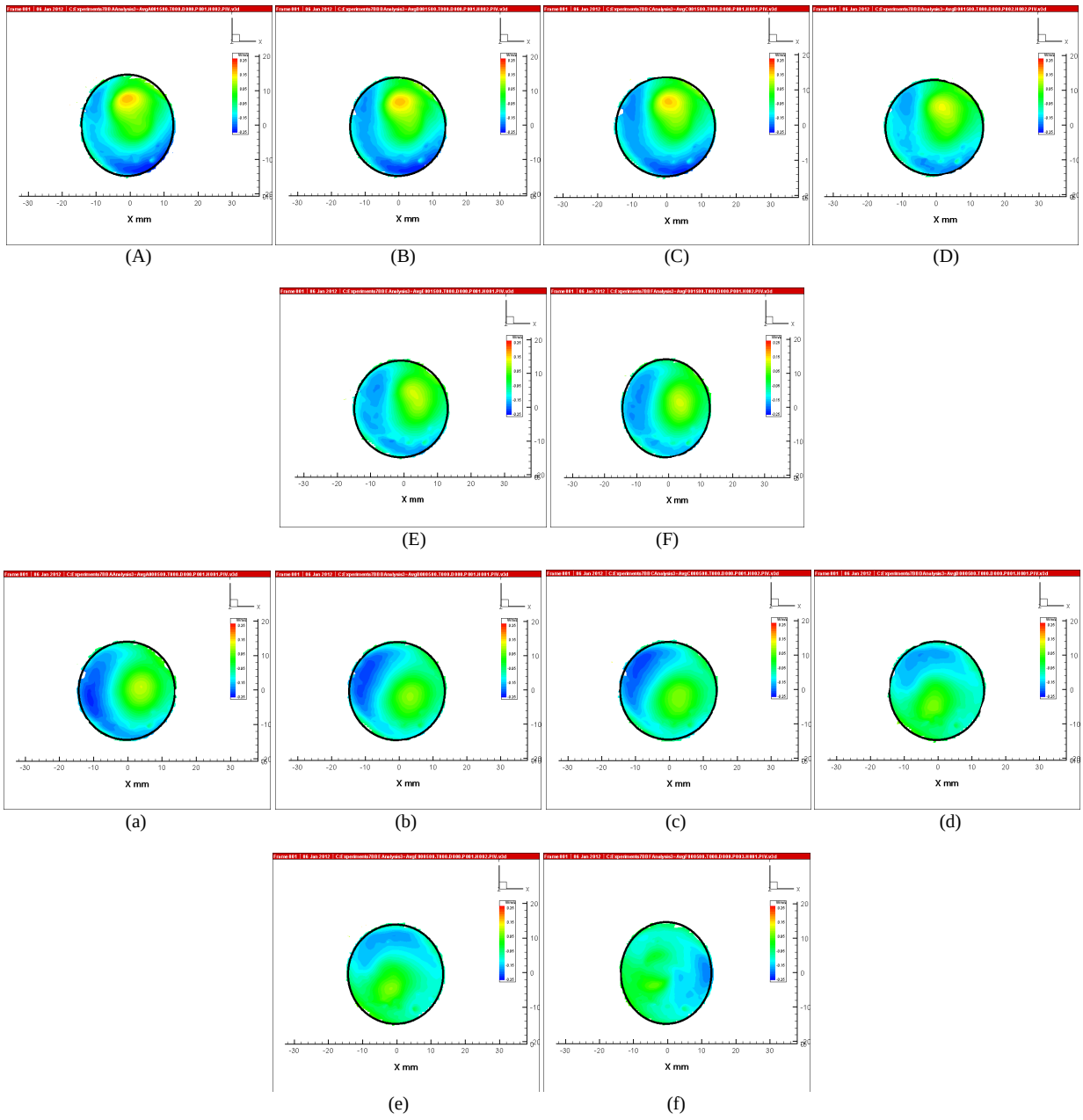

Figs. 8. Contour Plots of the Mean Axial Velocity for Water flow and Air-Water flow at Z= -395 mm axial position.
(A): $2.05\times10^{-4}m^3/s$ (water), $4.5\times10^{-5}m^3/s$ (air); (B): $1.96\times10^{-4}m^3/s$ (water), $4.5\times10^{-5}m^3/s$ (air); (C):$1.85\times10^{-4}m^3/s$ (water), $4.5\times10^{-5}m^3/s$ (air); (D):$1.58\times10^{-4}m^3/s$ (water), $4.5\times10^{-5}m^3/s$ (air); (E): $1.48\times10^{-4}m^3/s$ (water), $4.5\times10^{-5}m^3/s$ (air); (F): $1.32\times10^{-4}m^3/s$ (water), $4.5\times10^{-5}m^3/s$ (air);)
(a): $2.05\times10^{-4}m^3/s$ (water) (b): $1.96\times10^{-4}m^3/s$ (water) (c): $1.85\times10^{-4}m^3/s$ (water) (d): $1.58\times10^{-4}m^3/s$ (water) (e): $1.48\times10^{-4}m^3/s$ (water) (f): $1.32\times10^{-4}m^3/s$ (water)

IV. Conclusion

Air-water velocity measurements were conducted at three different axial positions for six different water flow rates and a constant air flow rate. The effect of air flow on the air-water velocity fields was established by comparing the air-water and water-only flow fields. The free vortex region of the tangential velocity profile begins at different values of radius for the air-water flow and this shows that the addition of air flow leads the core of the tangential velocity distribution within the pipe separator to be transient. The tangential and the radial velocity profiles of air-water flow are the same with that of water-only flow fields. However, the magnitude of the air-water velocity fields is observed to be higher than that of the water-only flow. The axial velocity plots of air-water flow field at Z=295 mm showed that most of the area of the contour plots are occupied by upward flow.

This means as air-water mixture enter the pipe separator, air separates and moves upward and flows out through the gas outlet of the pipe separator.

Acknowledgements

The authors thank EPSRC, TSI Inc for the useful support and discussions relevant to this work. The authors acknowledge funding from the Petroleum Technology and Development Fund (PTDF), Nigeria.

References

[1] Adrian R. J. Twenty years of particle image velocimetry. *Experiments in fluids, 39:2 (2005) 159-169.*

[2] Li, Ya-lin ; Yuan, Shou-qi ; Tang, Yue ; Yuan, Jian-ping, Motion of Tracer Particles in a Centrifugal Pump and its Tracking Characteristics, *Journal of Hydrodynamics, Ser.B, , Vol.24.5, (2012) pp.785-793.*

[3] Ragnid, S.F and Van Oudheusden, B.W; Particle tracer response across shock measured by PIV. *Experiments in fluids, 50:1 (2011) pp. 53-64.*

[4] Raffel, M., Willert, C. and Kompenhans, J. Particle Image Velocimetry: A Practical Approach. (Springer London 2007).

[5] Prasad, A. K. Stereoscopic Particle Image Velocimetry, *Experiments in Fluids, 29,*(2000) pp. 103 116.

[6] Liu, Z., Jiao, J., Zheng, Y., Zhang, Q. and Jia, L. Investigation of turbulence characteristics in a gas cyclone by stereoscopic PIV', *AIChE Journal, 52,* (12) (2006) pp. 4150-4160.

[7] Ng,I. Paganin, D.M and Fouras, A; Optimization of in-line phase contrast particle image velocimetry using a laboratory x-ray source , Journal of Applied Physics 112, (2012) 074701

[8] Bellani, G. Experimental Studies of Complex flow through Image-based Techniques. Royal Institute of Technology KTH, (2011) Stockholm, Sweden.

[9] Adrian, R. J. and Westerweel, J. *Particle Image Velocimetry* Cambridge University Press London 2011.

[10] Hassan, Y. A. 'Multiphase Bubbly Flow Visualization Using Particle Image Velocimetry', Annual New York Academy of Sciences, (2002) 972.

[11] Hassan, Y. A., Schmidl, W.D and Ortiz- Villafuerte, J. 'Three Dimensional Bubbly Flow Measurement Using PIV, *Journal of Visualization, 1,* 3 (1999) pp. 291 - 301.

[12] Liu, Hai-fei, Xu, Jing-yu and Zheng, Zhi-chu; Numerical study on oil and water two-phase flow in a cylindrical cyclone, *Journal of hydrodynamics 22:5 (2010) pp: 832-837.*

[13] Vazquez, C. O. *Multiphase flow separation in Liquid-Liquid cylindrical cyclone and Gas-Liquid -Liquid cylindrical cyclone compact separators* PhD dissertation, The University of Tulsa, USA 2001.

[14] Afolabi, E.A, *Experimental Investigation and CFD Simulation of Multiphase flow in a Three Phase Pipe Separator*. Ph.D dissertation. School of Chemical Engineering and Advanced Materials, Newcastle University, Newcastle, UK 2012.

[15] Reyes-Gutiérrez, M. A., Rojas-Solórzano, L. R., Colmenares, J., Marín-Moreno, J. C. and Meléndez-Ramírez, A. J. 'Eulerian-Eulerian modeling of disperse two- phase flow in a gas-liquid cylindrical cyclone,, *Journal of Fluids Engineering, Transactions of the ASME, 125,* (2006) pp. 832- 838.

[16] Barnea, D. A unified model for predicting flow-pattern transitions for the whole range of pipe inclinations, *International Journal of Multiphase Flow, 13,* 1 (1986) pp. 1-12.

[17] Perez, Valente Hernandez; *Gas-liquid two-phase flow in inclined pipes* Ph.D dissertation, The University of Nottingham 2007.

[18] Bergström, J. and Vomhoff, H. Experimental hydrocyclone flow field studies, *Separation and Purification Technology, 53,* 1 (2007) pp. 8-20.

[19] Concha, F. Flow Pattern in Hydrocyclones', *Kona-Powder and Particle, 25,* (2007) pp. 97-132.

[20] Fisher, M. J. and Flack, R. D. Velocity distributions in a hydrocyclone separator, Experiments *in Fluids,* 32, 3 (2002) pp. 302-312.

[21] Bai, Z. S., Wang, H. I. and Tu, S. T. Experimental study of flow patterns in deoiling hydrocyclone, *Minerals Engineering,* 22, 4 (2009) pp. 319-323.

[22] Peng, W., H, Dries, A.C, Regelink, M. and Foo, K. K. Reverse-flow centrifugal separators in parallel: Performance and flow pattern, *AIChE Journal, 53,* 3 (2007) pp. 589-597.

[23] Siangsanun, V., Guigui, C., Morchain, J., Marteil, P., Levecq, C., Puprasert, C. and Hébrard, G. Velocity measurement in the hydrocyclone by oil droplet, doppler ultrasound velocimetry, and CFD modelling, *Canadian Journal of Chemical Engineering, 89:4 (2011) pp. 725-733.*

[24] Dlamini, M. F., Powell, M. S. and Meyer, C. J. A CFD simulation of a single phase hydrocyclone flow field, *Journal of The South African Institute of Mining and Metallurgy, 105,* 10 (2002) pp. 711-717.

Authors' information

Eyitayo A Afolabi is a lecturer at the department of chemical engineering, federal University of Technology, Minna, Nigeria. He was graduated in 2005 as Chemical Engineer (M. Eng) at FUT, Minna, Nigeria. His PhD thesis is on Experimental Investigation and CFD Simulation of Multiphase flow in a Three Phase pipe Separator and was awarded by the University of Newcastle, Newcastle, UK in 2012. He is an affiliate member of the Institute of Chemical Engineers and academic partner of the Science, Chemical and Industry.
E-mail: elizamos2001@yahoo.com

Jonathan Lee is a Lecturer at the School of Chemical Engineering and Advanced Materials, Newcastle University, UK.
E-mail: j.g.m.lee@newcastle.ac.uk